Princeton Plasma Physics Laboratory

PPPL-4178

PPPL-4178

# Bispectral Analysis of Low- to High-confinement Mode Transitions in the National Spherical Torus Experiment

A.E. White, S.J. Zweben, M.J. Burin, T.A. Carter,
T.S. Hahm, J.A. Krommes, and R.J. Maqueda

June 2006

Prepared for the U.S. Department of Energy under Contract DE-AC02-76CH03073.

# Princeton Plasma Physics Laboratory
# Report Disclaimers

## Full Legal Disclaimer



## Trademark Disclaimer



# PPPL Report Availability

## Princeton Plasma Physics Laboratory

This report is posted on the U.S. Department of Energy's Princeton Plasma Physics Laboratory Publications and Reports web site in Fiscal Year 2006.

The home page for PPPL Reports and Publications is:

http://www.pppl.gov/pub_report/

## Office of Scientific and Technical Information (OSTI):

Available electronically at: http://www.osti.gov/bridge.

Available for a processing fee to U.S. Department of Energy and its contractors, in paper from:

U.S. Department of Energy
Office of Scientific and Technical Information
P.O. Box 62
Oak Ridge, TN 37831-0062

Telephone: (865) 576-8401

Fax: (865) 576-5728

E-mail: reports@adonis.osti.gov

# Bispectral analysis of low- to high-confinement mode transitions in the National Spherical Torus Experiment

A. E. White,[1] S. J. Zweben,[2] M. J. Burin,[3] T. A. Carter,[1]

T. S. Hahm,[2] J. A. Krommes,[2] and R. J. Maqueda[2]

[1]*University of California Los Angeles, Los Angeles, California 90095*[*]

[2]*Princeton Plasma Physics Laboratory, Princeton, New Jersey 08540*

[3]*Department of Astrophysical Sciences,*

*Princeton University, Princeton, New Jersey 08540*

(Dated: May 30, 2006)

## Abstract

This paper will present an experimental study of the temporal and spatial characteristics of the auto-bicoherence calculated from light amplitude fluctuations measured in the edge plasma of the National Spherical Torus Experiment (NSTX) [1] using data from the Gas Puff Imaging (GPI) diagnostic [2, 3] obtained during a series of thirteen shots in which the NSTX plasma underwent spontaneous low- to high-confinement mode (L-H) transitions. The auto-bicoherence calculated from the available GPI chord signals in the region near the magnetic separatrix and just above the outer midplane indicates that there is no significant increase, i.e. outside the R.M.S. error, in the amount of nonlinear coupling between low frequency fluctuations and high frequency fluctuations during the 10 ms before the transition. Limitations of bicoherence analysis are discussed.

PACS numbers:

[*]Electronic address: white@physics.ucla.edu

## I. INTRODUCTION

The spontaneous H-mode discovered in 1982 by the Axially Symmetric Divertor Experiment (ASDEX) team [4] is one of the most important operating regimes for tokamaks and stellarators. The mechanism that causes the tokamak plasma to undergo a transition from a regime of low confinement (L-mode) to a regime of high confinement (H-mode) is still not entirely understood. In the presently accepted model for the L-H transition, the turbulence is broken up by sheared poloidal flows, leading to a decrease in the fluctuation amplitude and a transient decrease in turbulent transport at the edge of the plasma [5]. This allows the pressure gradient to increase significantly leading to the transport barrier characteristic of the H-mode. The mechanism that generates and limits the sheared poloidal flows is still unknown. It has been proposed that the sheared flow can be generated in a self-organization process where the turbulence itself, through the Reynolds Stress, can drive the flows [6, 7].

Direct measurement of the Reynolds stress is difficult, but it has been done successfully on several tokamaks [5, 8, 9], although not during an L-H transition. To make a connection between the theory and a more experimentally accessible measurement, several authors have examined the problem in terms of a mode coupling model, in which the turbulent fluctuations transfer energy to large scale flows through three-wave interactions [7, 10]. It is possible to relate the bispectrum and the bicoherence to Reynolds Stress-generated shear flows via a mode coupling model [10]. This model shows that the auto-bispectrum calculated from a turbulent fluctuation measurement of ion-saturation current, $I_{sat}$, or floating potential, $V_f$, at one location can be used to measure the amount of coupling between low and high frequency fluctuations. The auto-bicoherence can be used to search for an increase in such coupling before an L-H transition. If such an increase were observed along with the formation of a shear layer, as occurs at the transition, this would be consistent with the Reynolds Stress-driven flow, or turbulence-driven flow, hypothesis for the L-H transition [10].

The bicoherence has been calculated during L-H transitions in the Wendelstein VII-AS stellarator [11] and also during biased H-mode operation in the Continuous Current Tokamak (CCT) [10]. The only previous bicoherence results obtained during a spontaneous L-H transition in a tokamak are from studies performed on DIII-D [12, 13]. A reciprocating Langmuir probe was used to measure fluctuations in the $I_{sat}$ or $V_f$ in the edge plasma during

an L-H transition [12] and it was reported that the amount of nonlinear coupling increased significantly just prior to the L-H transition when the probe was inside the separatrix [12]. This coupling was attributed to interactions between large scale fluctuations and small scale fluctuations, a result that is qualitatively consistent with the turbulence-driven flow hypothesis for the L-H transition [10, 12]. Motivated by the bicoherence study from the DIII-D tokamak using Langmuir probe data, this paper will describe a bicoherence study from the National Spherical Torus Experiment (NSTX) using the Gas Puff Imaging (GPI) diagnostic chord data.

We present a bicoherence study of the light amplitude fluctuations measured in the edge plasma of NSTX with the GPI diagnostic during thirteen discharges that underwent spontaneous L-H transitions. The auto-bicoherence from the available GPI chord signals in the region $\pm 5$ cm across the EFIT [14, 15] separatrix and just above the outer midplane indicates that no sudden increase in the amount of nonlinear coupling between low frequency fluctuations and high frequency fluctuations occurs within the 10 ms before the transition. Using the model from [10] as a basis for interpreting the auto-bicoherence, these results apparently indicate that coupling between turbulence and poloidal flows does not increase significantly in the edge immediately before the transition, at least in the region viewed by the GPI chords in this study.

A brief description of the GPI diagnostic is given in Section II. Section III introduces bispectral analysis and the specific definitions of the bicoherence that were applied to GPI chord data. Section IV contains a complete description of how the bicoherence calculations were carried out and the results from the NSTX GPI chord data. Section V discusses general limitations to the application of bicoherence analysis and limitations of the interpretation of GPI bicoherence results. Section VI provides ideas for future work. Section VII contains the summary and conclusions of this study.

## II. THE GAS PUFF IMAGING (GPI) DIAGNOSTIC ON NSTX

The Gas Puff Imaging (GPI) diagnostic on NSTX has been described in detail elsewhere [2, 3, 16] and only a brief overview is given here. For this study, $D_\alpha$ (656 nm) line emission from a deuterium gas puff is imaged along the magnetic field line direction at the plasma edge near the magnetic separatrix on the outboard side of NSTX ($R = 85$ cm, $a = 65$ cm).

Because the turbulent structures are highly elongated along the magnetic field lines, the GPI diagnostic views a poloidal and radial cross-section of the edge turbulence.

The GPI diagnostic can be used to study edge plasma turbulence due to fluctuations in electron temperature and density. The light emission at the $D_\alpha$ line occurs where $T_e \approx 5-100$ eV, spanning a region approximately $\pm 5$ cm across the separatrix. The amplitude of the light emitted at a given neutral density, $n_o$, is a nonlinear function of the local electron density, $n_e$, and electron temperature, $T_e$ [2, 3, 17]. The effects of such a nonlinear relationship on the interpretation of the bicoherence is discussed in section V H. It is noted that in general the $D_\alpha$ light emission amplitude depends on $n_o$, however, because of the gas puff strength used in this experiment, the turbulent fluctuations in the light amplitude will not depend on $n_o$.

The GPI diagnostic on NSTX produces two types of data. First, a PSI-5 fast-camera (250,000 frames/s for 1.2 ms) is used to make 2-D images of the turbulence in the poloidal and radial plane. Second, a separate array of 13 discrete views, which are commonly referred to as "chord" data, is used to obtain 1-D time-series data from the light amplitude fluctuations. The 1-D time-series data is digitized at 500,000 samples/s for 64 ms with an analogue bandwidth of 200 kHz. At the location of the gas puff, each chord views a 2 cm diameter section of plasma and the chord centers are spaced 2 cm apart. The radial GPI chord data spans roughly $\pm 5$ cm on each side of the separatrix. Figure 1 shows a still-frame image from the camera along with the discrete chord view positions that are located in the same $23 \times 23$ cm$^2$ field of view. The approximate position of the magnetic separatrix as inferred from EFIT, is also shown in figure 1. The auto-bicoherence in this study is calculated using the 1-D time-series chord data, not the 2-D camera data.

## III. BISPECTRAL ANALYSIS

### A. The auto-bispectrum and the auto-bicoherence

Bispectral analysis is a higher order statistical technique that is useful for studying systems that contain a quadratic nonlinearity [18–21]. The seminal paper for the use of bispectral analysis in plasma physics is Ref. [18]. That paper describes a basic algorithm for calculating the bispectrum using Fast-Fourier Transform (FFT) analysis. For a detailed

discussion of the FFT method of bicoherence calculations, Refs. [18, 20, 21] are recommended. Wavelet methods, which may have some benefits over FFT methods in studying the bicoherence, e.g. improved time resolution, have also been developed [11]. This paper will present auto-bicoherence results calculated using only the FFT method.

The auto-bispectrum is a third order spectral quantity. It is defined as an ensemble average,

$$B(k_1, k_2) = \langle \Phi(k_1)\Phi(k_2)\Phi^*(k_3) \rangle$$

where the triad of modes obeys the three-wave interaction criteria of conservation of momentum, namely that $k_1 + k_2 = k_3$. Here $\Phi(k)$ is the Fourier transform of a data signal in $k$-space, and $k_i$ is a wave number. The auto-bispectrum is a complex quantity and both its amplitude and its phase (known as the biphase) can be used in statistical studies of nonlinear interactions and phase coupling [22]. This paper will not address the use of the biphase to study nonlinear interactions.

The auto-bispectrum can be normalized in several ways to study different aspects of a time-series [19–21, 23]. For studying quadratic mode coupling the most commonly used normalization is the auto-bicoherence. The squared auto-bicoherence is defined as

$$b^2(k_1, k_2) = \frac{|B(k_1, k_2)|^2}{\langle |\Phi(k_1)\Phi(k_2)|^2 \rangle \langle |\Phi(k_3)|^2 \rangle}$$

According to this definition, the squared auto-bicoherence is bounded between 0 and 1, and is a quantitative measure of the amount of quadratic coupling between a triad of phase-coherent, or phase coupled, Fourier modes ($k_1 + k_2 = k_3$) in the system [10]. Three modes are phase coupled if the three signals maintain a fixed phase relation, such as $\phi_1 + \phi_2 = \phi_3$.

As the result of a nonlinear interaction, two waves could beat together to drive a perturbation, a third mode, that will be coupled to the first two modes. The bicoherence detects the phase coupling that occurs as the result of such an interaction. If the three modes are related via a nonlinear interaction then they will be phase coupled, and $b^2(k_1, k_2)$ will be near unity. If the phases of the three modes are not coupled, then the ensemble averaging in the bicoherence calculation will lead to a value of $b^2(k_1, k_2)$ near zero. If a third mode in the system is not the result of a nonlinear interaction, then it will have no fixed phase relationship with the other two modes in the system. The bicoherence will be zero for this case even if the third mode happens to satisfy $k_1 + k_2 = k_3$. For actual turbulent systems where the turbulence may be thought of as many modes interacting with each other, values

of $b^2(k_1, k_2)$ larger than 0.5 would indicate significant coupling [18, 20].

The auto-bispectrum has several symmetry properties that limit the domain over which it must be calculated [18]. Because of these symmetry properties, auto-bicoherence cannot be used to distinguish between a sum and a difference interaction. This means the auto-bicoherence does not indicate the direction of energy transfer. As developed by Ritz *et al.* [24, 25], further measurements and calculations using higher-order spectral analysis are needed to estimate the power transfer function in order to determine the direction of energy transfer. Recently a technique that is an extension of the Ritz method has been used on the H-1 toroidal heliac to experimentally identify the inverse energy cascade that results in large-scale turbulent structures such as zonal flows [26]. We note that the auto-bicoherence is only used in the GPI study as a measure of the relative strength of nonlinear interactions, and the results do not include information about the direction of energy transfer. All references to bicoherence or bispectrum from the GPI chord data in this paper refer to the auto-bispectral quantities calculated using just one time-series data set.

### B. The frozen flow hypothesis

The bicoherence of an experimentally measured fluctuating quantity, such as light amplitude, can be directly calculated using Fourier transforms in frequency space. In order to relate the bicoherence measuring coupling between frequencies to the bicoherence measuring coupling between wavenumbers, some information about the dispersion relationship $f(k)$ is needed. Using the the Frozen Flow Hypothesis (FFH), frequency and wavenumber can be directly related. The FFH assumes that the turbulence does not evolve significantly in the time it takes to pass by two spatially separated measurement points [10, 12]. From this assumption, a wavenumber, $k$, will be linearly related to a frequency, $f$. In this experiment it is the poloidal wavenumbers, $k_\theta$, that are of interest. The poloidal propagation time, $\tau$, is calculated from the separation between two poloidally spaced chords, $\delta x$, and the phase velocity of the fluctuating signal, $v_\theta$, where $\tau = \delta x / v_\theta$.

In the edge of NSTX, the poloidal $v_\theta$ is estimated using time-delay correlation analysis to be $v_\theta \sim 5$ km/s during both L-mode and H-mode [16], giving a propagation time $\tau \sim 5$ $\mu$s. The auto-correlation time of the turbulence , $\tau_A$, also determined from the chord data using time-delay correlation techniques, is $\tau_A \sim 24 - 32$ $\mu$s [3]. Because $\tau_A > \tau$, the FFH is

assumed to be valid in the poloidal direction for the edge turbulence in NSTX as measured by the GPI diagnostic [10, 12]. Some limitations and examples of how this hypothesis could fail are discussed in Section V C.

### C. Definition of bicoherence used to study NSTX GPI data

The bispectrum in frequency space is defined as

$$B(f_1, f_2) = \langle \phi(f_1)\phi(f_2)\phi^*(f_3) \rangle \tag{1}$$

with the associated bicoherence defined as

$$b^2(f_1, f_2) = \frac{|B(f_1, f_2)|^2}{\langle |\phi(f_1)\phi(f_2)|^2 \rangle \langle |\phi(f_3)|^2 \rangle}$$

Here $\phi(f)$ is the Fourier transform of the time signal at the mode frequency $f$ and the mode frequencies obey the three-wave interaction requirement, $f_1 + f_2 = f_3$, of conservation of energy.

Changes can be made to this normalization to correct for low power in the signal at any given frequency [19], and the effects of using the correction are discussed further in Section V. The bispectral analysis for this study was done using the low power correction (LPC) according to the following definition of the squared bicoherence

$$b^2(f_1, f_2) = \frac{|B(f_1, f_2)|^2}{\langle |\phi(f_1)\phi(f_2)|^2 \rangle \langle |\phi(f_3)|^2 \rangle + \epsilon} \tag{2}$$

where $\epsilon = [\min(\langle |\phi(f)|^2 \rangle)]^3$ [19].

From the squared bicoherence, two other useful values, the total bicoherence and the summed bicoherence, can be calculated [10, 11]. The summed bicoherence is a measure of the amount of coupling at the sum frequency $f_3$ relative to all other sum frequencies and is defined as

$$b^2(f_3) = \sum_{f_1 + f_2 = f_3} b^2(f_1, f_2) \tag{3}$$

The total bicoherence gives a measure of the total amount of coupling in the signal integrated over all frequencies and is defined as

$$b^2(t) = \sum_{f_1} \sum_{f_2} b^2(f_1, f_2) \tag{4}$$

The total bicoherence is used as a measure of total coupling at one time, $t$, chosen as the center of the time interval over which the ensemble average of equation (2) is calculated. We also define the average total bicoherence, which is the total bicoherence averaged over multiple NSTX shots, $s$,

$$\overline{b^2(t)} = \frac{1}{s}\sum_{i=1}^{s} b_i^2(t) \tag{5}$$

## IV. NSTX RESULTS

### A. Plasma parameters

The bicoherence results described in this paper were obtained from a sequence of thirteen discharges (#113732 − 113744) taken on one day with NSTX plasma parameters given in Table 1. All of these discharges had toroidal field $B_o = 3$ kG, $2 - 4$ MW of Neutral Beam Injection (NBI) power and underwent spontaneous L-H transitions that were captured by the chord data. For one discharge in this series the transition was captured by the fast camera as well. The L-H transitions studied in this paper are regular spontaneous transitions, i.e. they are not induced by sawtooth activity. The position of the separatrix, as determined from the latest version of EFIT, is located between $R = 147$ cm and $R = 150$ cm for the shots in this series. The position of the separatrix with respect to the radial chord positions is shown in Fig. 2. The poloidal chord array, centered at chord R4, is located slightly outside the separatrix for the shots analyzed in this paper.

Figure 2 shows GPI intensity profiles from time-averaged camera images for the discharges described in this paper. This intensity profile from the camera data is used to show the radial location of the chord views with respect to the peak in the light emission profile. Due to a slight nonlinearity in the camera that has been noted for data from this shot sequence [16], the actual light emission profile will be slightly different, but qualitatively similar, to the profile shown here. The edge plasma profiles for $n_e$ and $T_e$, also shown in Fig.2, come from Thomson scattering for four similar shots in this sequence, all taken ±8 ms with respect to the L-H transition [16].

### B. Spectral and Correlation Analysis

The GPI chord data measures fluctuations in the amplitude of the emitted $D_\alpha$ light, and the observed spectra are similar to those observed with other edge diagnostics such as Langmuir probes that measure $I_{sat}$ or $V_f$ [3]. In Fig. 3 part (a) the amplitude-vs-time trace from one chord shows how the signal amplitude of the GPI chords drops during the L-H transition. This is due to the region of light emission moving in at the transition as shown by the GPI camera intensity profiles in Figure 2. Figure 3 part (c) shows the $D_\alpha$ light emission trace. For each discharge, the time of the transition, $t_{LH}$, is determined by the drop in amplitude of the $D_\alpha$ trace. The signal amplitude of the GPI chords, shown in Fig. 3 part (a), typically decreases within 100-200 $\mu$s around $t_{LH}$, on a similar time-scale as the drop in amplitude of the $D_\alpha$ light emission trace.

Part (b) of Fig. 3 shows the power spectrum in time of the center GPI chord signal, R4. The light amplitude fluctuations have a broadband power spectrum, with lower power amplitude during H-mode. This is seen also in the average power spectra shown in Fig. 4. Figure 3 part (d) shows the power spectrum from the Mirnov coil signals. During the H-mode, a long lived coherent mode with frequency near 100 kHz is visible in the spectrum of the chord data for all the shots analyzed. This mode also appears in the spectrum of the Mirnov coil signals and it was reported previously that this mode frequency occurs in the toroidal Alfven frequency gap [27]. Since this mode does not appear before the transition it is probably not related to any precursor dynamics as studied in this paper.

The spatial and temporal structure of the turbulence can be investigated using the 2-D camera data or by using time-delay correlation analysis of the chord data to calculate the radial and poloidal correlation lengths and auto-correlation time of the turbulence. Typical auto-correlation times of 24-32 $\mu$s are observed [3]. Typical average poloidal correlation lengths are $L_{pol} = 6.8\pm1.5$ cm and typical average radial correlation lengths are $L_{rad} = 4.8\pm1$ cm, and it is observed that there is no significant difference between the correlation lengths calculated from GPI data before and after the L-H transition [16].

In NSTX the H-mode plasmas are distinguishable from L-mode plasmas [28] and the NSTX H-mode plasmas are similar to H-mode plasmas in conventional aspect-ratio tokamaks [29]. The recent NSTX GPI study by Zweben *et al.* [16] indicates that at the L-H transition in NSTX the correlation lengths do not significantly change and the gradient in the poloidal

flow of the turbulence itself does not increase, at least in the region near or just outside the separatrix. However, since the ExB fluid flow was not directly measured in this region, no quantitative comparison of these results with the conventional ExB flow shear model has yet been made.

### C. Calculating bicoherence during the L-H transition

The goal of this study is to compare the bicoherence before and after the L-H transition on NSTX, and especially to investigate if any sudden increase in the bicoherence occurs immediately prior to the transition . Several properties of data signals in general can lead to false positive and negative results in bicoherence analysis, and the details will be discussed in Section V.

In order to avoid false bicoherence results we avoid two portions of the raw data, (i) during L-mode the roughly 100-200 $\mu$s of data at the transition where a sharp decrease in GPI chord signal amplitude occurs and (ii) during H-mode the portions of the data where an ELM-type event or brief return to L-mode occurs. Figure 3 shows one example of the portions of the GPI chord signals that were used to reliably calculate the bicoherence: for shot #113741 the interval of L-mode data from $170 - 190.5$ ms and the interval of data in H-mode from $190.7 - 200$ ms are used. Typical data lengths are $10 - 30$ ms during the L-mode portions of the shots, and $5 - 10$ ms during the early H-mode portion of the shots.

The portions of the data during L-mode and during H-mode are then divided up into several time intervals, which are each divided into records. The bicoherence is calculated as an ensemble average in time over these records using equation (2). The statistical significance level of the bicoherence is estimated as $1/M$ where $M$ is the number of records [12, 30]. A bicoherence value below the significance level means that any bicoherence values caused by nonlinear coupling are of too low amplitude to be distinguished from random peaks caused by statistical noise, and the values below the statistical significance level can be taken to mean no coupling. When using 4.086 ms time windows divided into 16 records of 128 points, the frequency resolution is $\delta f \sim 4$ kHz and the statistical significance level is $1/M = 0.0625$. In some of the bicoherence calculations described below, different window lengths or a different number of records were used. When this is done we find that the general trends in the bicoherence do not change. A short discussion of the convergence of the bicoherence is given

in Section V.

### D. Bicoherence results for a typical NSTX shot.

Bicoherence results from one chord for one of the thirteen shots will be described in detail as an example of the general trend seen in all NSTX GPI data. Chord R4 is the center view in the array located at major radius $R \approx 150$ cm as shown in Fig. 2. This chord is the working chord closest to the separatrix during all the shots in the series. Although it may be viewing a region that is located slightly outside the separatrix, the light amplitude fluctuations seen in the chord R4 signal do change qualitatively at the transition. The results of calculating the total bicoherence, squared bicoherence and summed bicoherence from chord data using the shot, #113739 are described below.

Figure 5 shows the contour plots of squared bicoherence, $b^2(f_1, f_2)$, at six different times during L-mode and H-mode for shot #113739 using the signal from chord R4. Each contour of $b^2(f_1, f_2)$ is calculated from a 4.086 ms time window before or after the transition. The number of records used in each time window was 16 and only the $b^2(f_1, f_2)$ values that are above the statistical significance level, $1/M \approx 0.06$, are shown in the contours.

The contour plots show what frequencies take part in the coupling before and after the L-H transition. Typical of all thirteen shots analyzed, the coupling during L-mode occurs fairly evenly over all frequencies, and no increase in the $b^2(f_1, f_2)$ is seen prior to the transition. After the transition, coupling becomes localized to frequency triads such that $f_1$ and $f_2$ are below 100 kHz. A peak in $b^2(f_1, f_2)$, can be interpreted in one of two ways, (i) as the result of a sum interaction between two low frequency modes, where $f_1,\ f_2 < 100$ kHz interact to give a peak at $f_1 + f_2 = f_3$, or (ii) as the result of a difference interaction between a high frequency mode and a low frequency mode, where $f_1 > 100$ kHz and $f_2 < 100$ kHz interact to give a peak at $f_1 - f_2 = f_3$.

The summed bicoherence, $b^2(f_3)$, calculated from equation (3) is another way of comparing the coupling in L-mode with that of H-mode. Figure 6 shows the coupling in shot #113739 occurring mostly at low sum frequencies ($f_3 < 100$ kHz) during H-mode while coupling is spread out among all sum frequencies during L-mode. The curves of $b^2(f_3)$ shown here were calculated using a 8.192 ms time window before and after the transition. The number of records used in each time window was 32 and the number of points in each record

was 128. The statistical significance level is $1/M \approx 0.03$. During H-mode the summed bicoherence for sum frequencies above 100 kHz drops below the statistical significance level.

The total bicoherence, $b^2(t)$, calculated from equation (4) is used to show temporal changes in the coupling across the L-H transition. For shot #113739, values of total bicoherence, $b^2(t)$, are plotted versus time in Fig. 7. The horizontal line in Fig. 7 represents the statistical significance level, $1/M \approx 0.06$. Here the number of records used in each 4.096 ms window is 16 and the number of points in each record is 128. For this shot the L-H transition time is $t_{LH} = 199$ ms. The last window before the transition extends from $t = 194.9$ ms to $t_{LH}$, and then the first window after the transition extends from $t = 199.1$ ms to $t = 203.2$ ms. The total bicoherence does not increase during the 10 ms prior to the L-H transition.

Each value of total bicoherence has been assigned to the time point at the center of the time window over which the ensemble average of the squared bicoherence was calculated. The points are separated by 0.2 ms, where the total bicoherence at each point is independently calculated from a 4.096 ms time window, and then the window is advanced in the raw data by 0.2 ms and another independent value of the total bicoherence in obtained. For this shot, and for all shots in this study, no significant increase in the total amount of coupling is seen during the 10 ms before the transition.

### E. General bicoherence results for multiple NSTX shots

The total bicoherence, squared bicoherence and summed bicoherence were calculated for each chord for all the shots in the series. After individually analyzing all thirteen shots in this study, it is expected that any general trend in the nonlinear coupling can be seen by averaging the results from total bicoherence calculations for all the shots.

For each shot, total bicoherence, $b^2(t)$, is calculated from equation (4) using 4.096 ms time windows, 16 records, and 128 points per record. Then the average total bicoherence for all the shots, $\overline{b^2(t)}$, is calculated from equation (5). Figure 8 shows $\overline{b^2(t)}$ relative to the L-H transition time for chord R4 data from all thirteen shots in the sequence. The error bars represent the the standard error, that is, the R.M.S error in the mean of the average total bicoherence, calculated for each time point from the average over multiple shots. This average bicoherence result indicates there is no statistically significant increase in the aver-

age amount of coupling at chord R4 within the 10 ms before the transition.

Using a smaller window length to improve the time resolution of the bicoherence calculation near the L-H transition, the same averaging over all thirteen NSTX shots is performed using the chord data from R4. Here each time window was taken to be 2.048 ms long and was divided up into 16 records of 64 points each. These smaller record lengths result in a frequency resolution of $\delta f \sim 8$ kHz. This mean total bicoherence this way is shown in Fig. 9, and no increase in the amount of coupling is seen in the 10 ms prior to the L-H transition. A slight increase in coupling appears more than 10 ms prior to the transition and is explored below further by examining five shots that have data during L-mode extending more than 20 ms before the transition.

The five of the NSTX shots that show a slight increase in the coupling more than 10 ms before the transition, shots # 113732, 113733, 113739, 113741, and 113744, have data during L-mode extending more than 20 ms before the transition. Figure 10 (a) shows the total bicoherence calculated for one of these shots, # 113741. The increase in the total bicoherence values appears at $t \approx 15$ ms before the transition in this shot, when the spread in the values also increases. These changes were not seen in shots that had shorter data lengths in L-mode. Shown in Fig. 10 (b) the average total bicoherence calculated using the above five shots indicates that in general the average values of the total bicoherence increase by 50% from $\overline{b^2(t)} \approx 0.1$ to $\overline{b^2(t)} \approx 0.15$ about 15 ms prior to the transition. This increase is within R.M.S. error. The average total bicoherence values tend to remain near $\overline{b^2(t)} \approx 0.15$ during the last 10 ms before the transition. As Fig. 10 (b) indicates, the slightly increasing linear trend in total bicoherence values seen in Fig. 10 part (a) for shot # 113741 lies almost entirely within the R.M.S. error for the five shots.

### F. Poloidal and radial bicoherence profiles

The NSTX GPI diagnostic provides a radial and a poloidal array of data near the separatrix. The radial and poloidal profiles of the bicoherence calculated using the L-mode portions of shots # 113732, 113733, 113739, 113741, 113744 are shown in Fig. 11. The R.M.S. error for the average total bicoherence values in the radial and poloidal profiles is $\delta b^2 \sim 15 - 30\%$, the same as for the average total bicoherence values shown in Fig. 10, but the error bars are not plotted on the profiles for clarity.

Figure 11 (a) shows the poloidal profile at four different times during L-mode. The poloidal position is determined as the distance from the center chord view, R4, located at major radius $R \approx 150$ cm as shown in figure 2. Little change is seen in the average total bicoherence calculated at different poloidal positions during L-mode during the 10 ms before the transition.

The radial profile is shown in Fig. 11 (b). The radial profile indicates a trend of increasing bicoherence with radius. The two chord views that are inside the separatrix, R1 and R2, have very low values of average total bicoherence. These two chords also do not show any increase in the bicoherence during the 10 ms prior to the L-H transition. The two chord views that are farthest outside the separatrix have the highest values of average total bicoherence. The bicoherence of these outer chords, R6 and R7, appears to decrease during the 10 ms prior to the L-H transition. The outer-most chords, R6 and R7, were in the scrape-off-layer (SOL) and the data is intermittent. The data from chords R3 at $R \approx 148$ cm and R5 at $R \approx 152$ cm had signal to noise ratios (SNR) that were lower than acceptable for bicoherence calculations, making the data unusable. The effects of intermittent signals and SNR on the bicoherence is discussed in Section V.

## V. DISCUSSION

### A. Convergence of the bicoherence estimator

When the variance of the bicoherence, given as $\mathrm{var(b)} \approx \frac{1}{M}[1 - b^2]$ [18], approaches zero, then the $b^2(f_1, f_2)$ has converged to its "true" value. In the case where a signal has strongly coupled discrete modes at many frequencies, typical bicoherence values are $b^2(f_1, f_2) \sim 1$. In this case as few records as $M = 16$ are needed to obtain a relative variance of 3%. However, in the case with broadband signals where $b^2(f_1, f_2) \ll 1$ for most frequencies, many more records are needed to obtain convergence. It has been shown in a specific experimental case with broadband data signals that in order to obtain a relative variance of 1% the number of records needed is $M \geq 500$ if $b^2(f_1, f_2) = 0.04$ [31]. The bicoherence is a statistical estimator, and due to the small number of records used in this study of broadband fluctuation data, the bicoherence values have probably not converged [12, 20, 30].

In the previous work from DIII-D [12] it has been noted that the location in frequency

space and the changes in total bicoherence amplitude, rather than the absolute amplitude, are important for studying gross features of the temporal coupling trend. Using closely spaced identical time interval lengths during the shot and averaging over multiple shots we can obtain information about gross trends in the total bicoherence from the NSTX GPI chord data. We have calculated the bicoherence using several different FFT record lengths, numbers of records and time window lengths for thirteen shots and have found that the reported trend in the total bicoherence of the GPI data is robust to these changes in statistics.

### B. Effect of the GPI nonlinear density response on bicoherence

It has been determined that the amplitude of GPI light fluctuations, $S$, is related to the electron density and temperature nonlinearly via $S \propto n_o f(n_e T_e)$ where $S$ is a monotonically increasing function [17]. To investigate the possibility that the coupling is occurring in the turbulent fluctuations of electron density but is not detectable in turbulent fluctuations of the light emission due to the nonlinear relationship, simple test signals were created. Figure 12 shows the changes in the bicoherence of a test signal composed of three sinusoids as the nonlinear relationship is varied. A test signal, $x$, where $x$ is a sum of three sinusoids, is operated on with the nonlinear function $y = x^\alpha$ where the nonlinear factor is varied, i.e. $\alpha = 0.1 - 2.2$. The squared bicoherence, $b^2(f_1, f_2)$, is calculated from $y$ and is evaluated at the frequencies where the test signal has quadratic coupling built into it, at $f_1 = 220$ Hz and $f_2 = 375$ Hz. The $b^2(220, 375)$ does not vary substantially as $\alpha$ deviates from unity. The total bicoherence, however, appears to increase as $\alpha$ deviates from unity. This is because the nonlinear relationship $y = x^\alpha$ introduces new modes that are phase coupled to the original signal, and this leads to a larger value of the total bicoherence than would be seen in $x$ alone.

This simple test indicates that coupling information about the underlying density fluctuations will still be present in the final coupling measured in the GPI signal, but that the absolute values of coupling from the GPI signal will be different than those from a pure density signal. The changes in $b^2(f_1, f_2)$ and in $b^2$ are valid indicators of changes in underlying coupling properties of the plasma turbulence. There are nonlinear effects in $I_{sat}$ fluctuation measurements from Langmuir probes as well [32], and these may also have to be taken into

account when calculating the bicoherence.

### C. Limitations of the frozen flow hypothesis

The frozen flow hypothesis (FFH) maintains that the spatial structure of the turbulence does not evolve significantly in the time it takes to pass by two spatially separated measurement points [10, 12]. The FFH is an essential assumption if one wants to interpret the frequency coupling as wavenumber coupling in the plasma. However, when calculating bicoherence in a region where the plasma flow pattern may be in both the radial and poloidal, $\theta$, directions, the FFH fails. For example, if the plasma flow is predominantly in the radial direction, then the FFH fails to hold in the poloidal direction because the poloidal phase velocity, and the propagation time, go to zero. This is a serious failure if the coupling in $f$ is intended to be interpreted solely as coupling in $k_\theta$. Furthermore, it is unclear when using turbulence measurements from only one spatial location to calculate the auto-bicoherence whether the FFH requires a physical flow to exist in the system, or whether it only requires the auto-correlation time of the turbulence to be longer than the time during which the fluctuations are measured.

### D. Avoiding false positives

The bicoherence calculated across a step-function or a delta function in uncoupled test signals will return a false positive. If the FFT is applied to a step function or to a delta function, then many phase coherent sinusoids are used. In this case the bicoherence will have a spuriously large value that cannot be distinguished from values associated with real coupling in the physical system.

If any of the records used in the ensemble average overlap the sudden decrease in GPI signal amplitude at the transition as seen in Fig. 3 (a), then the bicoherence value will be artificially high. This type of false positive was avoided in the NSTX results.

The chords that view areas of the plasma edge that are in the SOL have very short-time duration intermittent "spikes" in the signal that are believed to be related to radially and poloidally moving structures or "blobs"[3]. Some authors have noted that the bicoherence is not useful for studying intermittent or transient events because the bicoherence cannot

distinguish between a structure moving past a measurement point, seen as a spike in the data, and wave-wave coupling happening on a fast time scale [11]. Regardless of whether or not coupling is present, an isolated spike in the data will cause a large value of the bicoherence. If a few isolated spikes are present, they can be avoided. If the data is by nature intermittent, as in the SOL, then the bicoherence values cannot be interpreted directly as a measure of underlying coupling because the bicoherence is also measuring the presence of the many intermittent "spikes" in the signal.

### E. Motivation for using the low power correction

The low power correction (LPC) is used in equation (2) to calculate the bicoherence of NSTX GPI data in this study. The effects of the LPC on the bicoherence of actual GPI data is shown in Fig. 13. To calculate the bicoherence results presented in this paper, we wrote an analysis routine in the Interactive Data Language (IDL) called BISPEC following the algorithm outlined in Ref. [18]. Here the bicoherence is calculated using BISPEC (with and without the LPC) and is compared to the bicoherence calculated using the commercially available bispectral analysis package for MATLAB (the package does not implement the LPC) for several sections of shot #113741. The LPC suppresses false positives but does not affect bicoherence values associated with actual coupling seen from the two data points in the data interval t$\sim 180 - 190$ ms from Fig. 13.

Calculating the bicoherence for test signals indicates that the LPC suppresses the high bicoherence values associated with false positives. This can be seen in figure 14. The test signals shown here were constructed to have no coupling. When using the LPC, the bicoherence from these test signals drops below the statistical significance level. Also, the large values of the bicoherence associated with "false positives" due to signal amplitude changes or delta-function type "spikes" have been suppressed by using the LPC.

### F. Avoiding false negatives

Because the bicoherence, equation (2), is an ensemble average, it cannot resolve coupling happening on a time scale that is fast compared to the time interval associated with the number of points used in each record. If the coupling occurs only during some small fraction

of the FFT record time used for the ensemble average, then it is possible that the coupling will be averaged out over the larger window. Analysis of the GPI data was done with varying window and record lengths and in no case was any deviation from the reported trend seen.

The bicoherence is affected by the ratio of fluctuation to random noise levels, or the signal to noise ratio (SNR), of the data. The SNR of the GPI chord data drops from values greater than 25 during the L-mode to values between 7 and 10 during the H-mode. Generating test signals with perfectly coupled sinusoids and calculating the bicoherence reveals that a SNR below 5 will result in the bicoherence being unable to detect coupling in perfectly coupled test signals, as shown in Fig. 15. The SNR of the GPI data was certainly high enough during L-mode to reliably use the chord data to detect any increases in the coupling prior to the L-H transition. The low values of total bicoherence during H-mode may possibly be linked to the relatively low SNR of the chord data during H-mode.

### G. Interpretation of the radial bicoherence profile

The spatial localization of any increase in coupling that might occur during an L-H transition has not been predicted for NSTX. The results of the work on DIII-D show that the increase in bicoherence may be localized within millimeters of the separatrix [12] . The location of the separatrix as determined from EFIT for this series of discharges is between $R = 147$ and $R = 150$ cm. The radial range of data spans up to $\pm 5$ cm across this region. If the increase in coupling does occur in a relatively small radial region inside the separatrix, it could mean that the GPI chord data array did not capture the increase in coupling because the viewing region of R4 is too far outside the separatrix and the viewing region of R2 is too far inside the separatrix. For this series of shots, chord R3 is located at R= 148 cm but unfortunately the SNR of the data from R3 was too low to be used for bicoherence analysis.

The other reason that a very large increase in coupling prior to the transition may not be present in the region near the separatrix is that the shear flows might be generated much farther inside the separatrix prior to the L-H transition, at a radial location beyond the range of neutral gas penetration. The results from the GPI chords do show that there is a significant reduction in the bicoherence amplitude after the L-H transition and that there are differences in the location of coupling in frequency space before and after the transition. Therefore, although the bicoherence does not measure increased coupling as a precursor

to the L-H transition, the bicoherence does identify local changes in coupling, and these changes may be a result of nonlocal causes. This agrees with qualitative impressions from the 2-D GPI camera data, where there is no obvious precursor to the L-H transition in the field of view [16].

Another issue regarding the interpretation of the radial bicoherence calculations are the probability distribution functions, or PDFs, of the radial chord data. If a signal has a Gaussian PDF then the bispectrum will approach zero [18, 20]. The outermost radial GPI signals and the signals from chord R4, which was used predominantly in this study, have non-Gaussian PDFs, however, the innermost radial GPI signals typically have Gaussian PDFs [3]. It is expected that the bicoherence of these innermost radial chords should be quite low, while the bicoherence of the outer chords will be higher. This agrees with the radial bicoherence profile results.

### H. Using auto-bicoherence to detect coupling between turbulence and flows

While there appears to be agreement that the Reynolds Stress can generate mean flows in plasmas [5, 7, 10, 33–36] there is some disagreement in the literature as to the usefulness of the auto-bicoherence as a measure of the nonlinear coupling associated with detecting these turbulence-driven flows. Some authors have performed simulation studies that show that the auto-bicoherence from either $V_f$ or $I_{sat}$ measurements can be used to measure shear flow generation from turbulence [7, 35]. Other authors have performed simulation studies that indicate that the auto-bicoherence is not a useful measure of turbulence generated flows, and instead one needs the cross-bicoherence or direct Reynolds Stress measurements [37, 38].

Due to this disagreement, the interpretation of high values of the auto-bicoherence as direct evidence of nonlinear coupling between turbulence and flows is not a simple matter. This is true for the auto-bicoherence calculated from Langmuir probe data or GPI chord data. Previous auto-bicoherence studies have assumed that the auto-bicoherence can be used to measure nonlinear coupling associated with turbulence-driven flows during L-H transitions [10, 12]. In order to relate the results from NSTX to previous experiments, we use the same assumption. The disagreement as to the validity of this assumption is noted as a general limitation of bicoherence studies of turbulence-driven flows in plasma.

## VI. FUTURE WORK

The GPI diagnostic on NSTX provides an opportunity to study the spatial localization of quadratic nonlinear coupling in edge turbulence by using bispectral analysis of data obtained simultaneously at multiple locations near the separatrix. Four ideas for improving and adding to the present study are discussed below.

First, the wavelet bicoherence method could be used to improve the time resolution of the bicoherence analysis [11]. This could help in determining the time scales over which the coupling occurs. Using either wavelet or FFT methods, the slight increase in total bicoherence long before the transition could be studied further.

Second, more data from radial chords that are viewing the region near the separatrix during L-H transitions could be obtained from future NSTX runs in an attempt to determine if an increase in the coupling is only happening in a very small region not viewed by the GPI diagnostic in this study. However, the GPI camera image analysis indicates no increase in the poloidal flow speed of the turbulence at the transition, including through the region that is viewed by the chord that was not available for this study, chord R3 [16].

Third, this paper only describes auto-bicoherence results, and the cross-bicoherence could be calculated using the 2-D poloidal and radial array of fast-time series chord data. The cross-bicoherence is calculated using two different time-series data sets, in this case, it could be calculated using data from two spatially separated measurement locations. This quantity might yield different information about the nonlinear coupling.

Fourth, the experimental results of this study could be compared to simulations of the GPI experiments [17]. This may help in predicting the coupling properties of the turbulence as measured by the GPI diagnostic on NSTX.

## VII. SUMMARY AND CONCLUSIONS

The first trend observed in this study is that the auto-bicoherence from all available chord signals in the region $\pm 5$ cm across the EFIT separatrix and just above the outer midplane in NSTX indicates that no significant and sudden increase in the amount of nonlinear coupling between low frequency fluctuations and high frequency fluctuations occurs within the 10 ms before the transition for all of the thirteen shots studied. Because the past work on

DIII-D reported a large increase in the total amount of nonlinear coupling prior to the L-H transition only when the measurement was made 3 mm inside the separatrix in the highest gradient region [12], an important point to note when comparing the NSTX result to the DIII-D result is that a GPI chord signal was not available for chord R3. Chord R3 was likely viewing the highest gradient region during this study. However, an analysis of the poloidal flow velocity as a function of radius passing right through the viewing region of chord R3 was done using the NSTX GPI 2-D camera images and found no increase in the shear flow of the turbulence itself from L-mode to H-mode in the viewing region of the chords [16]. This suggests that the bicoherence behavior in the region viewed by chord R3 would not be different from that of any of the other chords.

A second trend, observed in five of the thirteen shots that had L-mode data extending 20 ms before the transition, is that approximately 15 ms before the transition the average total bicoherence values increase by 50% and remain at that level during the last 10 ms before the transition. This increase lies within the R.M.S. error calculated from the five shots and was not seen in the other eight shots in the series that had shorter data lengths before the transition.

A third trend is that the values of total bicoherence increase as radius increases. This is consistent with the radial changes in the PDFs of the radial chord data – the PDFs become more Gaussian deeper in the plasma and the bicoherence of a time-series approaches zero as the PDF becomes more Gaussian. The total amount of coupling is independent of the poloidal position, as is expected because these chords are at nearly the same poloidal angle.

A fourth trend observed is that during L-mode the amplitude of the total amount of coupling remains fairly constant and the peaks in coupling are spread out evenly among all frequencies, but during H-mode the total amount of coupling is found to decrease following the L-H transition, with peaks in the coupling becoming localized to frequencies below 100 kHz during H-mode. The previous bicoherence study on DIII-D also reported such a shift in coupling towards low sum frequencies [12].

In conclusion, we have presented a study of the temporal and spatial characteristics of the auto-bicoherence during thirteen discharges that underwent spontaneous L-H transitions in NSTX. The auto-bicoherence is calculated from light amplitude fluctuations measured in the edge plasma with data from ten of the thirteen GPI diagnostic chords. The main result is that the auto-bicoherence does not significantly increase during the last 10 ms prior to

the transition. We have discussed general limitations of the analysis as well as those specific to the GPI diagnostic. This bicoherence study of the L-H transition on NSTX could be most improved through the use of bispectral analysis beyond the auto-bicoherence and by obtaining chord data from the highest gradient region.

**Acknowledgments**

We are grateful to the NSTX team for their support for this experiment. Special thanks to George Tynan for his insightful comments and to John Menard for the EFIT results. Thanks also to Chris Holland and Brian Brugman for useful discussions. A.E.White′s work on this project was completed under appointment to the Fusion Energy Sciences Fellowship Program administered by Oak Ridge Institute for Science and Education under a contract between the U.S. Department of Energy and the Oak Ridge Associated Universities.

---

[1] M. Ono, M. G. Bell, R. E. Bell, and *et al.*, Plasma Physics and Controlled Fusion **45**, A335 (2003).

[2] R. J. Maqueda, G. A. Wurden, D. P. Stotler, and *et al.*, Rev. of Sci. Instr. **74**, 2020 (2003).

[3] S. J. Zweben, R. J. Maqueda, D. P. Stotler, and *et al.*, Nucl. Fusion **44**, 134 (2004).

[4] F. Wagner, G. Becker, K. Behringer, and *et.al.*, Phys. Rev. Lett. **49**, 1408 (1982).

[5] J. W. Connor and H. R. Wilson, Plasma Physics and Controlled Fusion **42**, R1 (2000).

[6] P. H. Diamond and Y. B. Kim, Phys. Fluids **3**, 1626 (1991).

[7] P. H. Diamond, M. Rosenbluth, E. Sanchez, C. Hidalgo, B. V. Milligan, T. Estrada, B. Branas, M. Hirsch, H. J. Hartfuss, and B. A. Carreras, Physical Review Letters **84**, 4842 (2000).

[8] C. Hidalgo, C. Silva, M. Pedrosa, E. Sanchez, H. Fernandez, and C. Varandas, Phys. Rev. Lett. **83**, 2203 (1999).

[9] G. S. Xu, B. N. Wan, M. Song, and J. Li, Phys. Rev. Lett. **91**, 125001 (2003).

[10] G. R. Tynan, R. A. Moyer, M. J. Burin, and C. Holland, Phys. Plasmas **8**, 2691 (2001).

[11] B. P. VanMilligan, E. Sánchez, T. Estrada, C. Hidalgo, B. Branas, B. Carreras, and L. García, Phys. Plasmas **2**, 3017 (1995).

[12] R. A. Moyer, G. R. Tynan, C. Holland, and M. J. Burin, Physical Review Letters **87**, 135001

(2001).

[13] R. Moyer, D. H. Lehmer, T. E. Evans, R. W. Conn, and L. Schmitz, Plasma Phys. Control. Fusion **38**, 1273 (1996).

[14] L. L. Lao, H. S. John, R. D. Stambaugh, A. G. Kellman, and W. Pfeiffer, Nuclear Fusion **25**, 1611 (1985).

[15] S. Sabbagh, S. Kaye, J. Menard, and *et al.*, Nuclear Fusion **41**, 1601 (2001).

[16] S. J. Zweben, R. J. Maqueda, J. L. Terry, and *et al.*, *Structure and motion of edge turbulence in the National Spherical Torus Experiment and Alcator C-Mod* (to be published in Phys. of Plasmas, 2006).

[17] D. P. Stotler, D. A. D'Ippolito, B. LeBlanc, R. J. Maqueda, J. R. Myra, A. A. Sabbagh, and S. J. Zweben, Contributions to Plasma Phys. **44**, 294 (2004).

[18] Y. C. Kim and E. J. Powers, IEEE Transactions on Plasma Science **7**, 120 (1979).

[19] W. B. Collis, P. R. White, and J. K. Hammond, Mechanical Systems and Signal Processing **12**, 375 (1998).

[20] J. W. A. Fackrell, S. McLaughlin, and P. R. White, Applied Signal Processing **3**, 155 (1995).

[21] J. W. A. Fackrell, S. McLaughlin, and P. R. White, Applied Signal Processing **2**, 186 (1995).

[22] K. Itoh, Y. Nagashima, S.-I. Itoh, P. H. Diamond, A. Fujisawa, M. Yagi, and A. Fukuyama, Physics of Plasmas **12**, 102031 (2005).

[23] M. J. Hinich, J. Time Series Analysis **3**, 186 (1982).

[24] C. P. Ritz, E. J. Powers, R. W. Miksad, and R. S. Solis, Phys. Fluids **31**, 3577 (1988).

[25] C. P. Ritz, E. J. Powers, and R. D. Bengston, Phys. Fluids B **1**, 153 (1989).

[26] H. Xia and M. G. Shats, Phys Rev. Letters **91**, 155001 (2004).

[27] R. Maingi, M. G. Bell, R. E. Bell, and *et al.*, Nuclear Fusion **43**, 969 (2003).

[28] S. M. Kaye, C. E. Bush, E. Fredrickson, B. LeBlanc, R. Maingi, and S. A. Sabbagh, Phys. Plasmas **10**, 3953 (2003).

[29] R. Maingi, M. G. Bell, R. E. Bell, and *et al.*, Phys. Rev. Letters **88**, 035003 (2002).

[30] D. Gresillon and M. S. Mohamed-Benkadda, Phys. Fluids **31**, 1904 (1988).

[31] M. J. Burin, Ph. D. thesis, University of California, San Diego (2003).

[32] I. H. Hutchinson, *Principles of Plasma Diagnostics* (Cambridge University Press, 1992).

[33] G. R. Tynan, M. J. Burin, C. Holland, G. Antar, and P. Diamond, Plasma Phys. Controlled Fusion **46**, A373 (2004).

[34] P. H. Diamond, Y. M. Liang, B. A. Carreras, and P. W. Terry, Physical Review Letters **72**, 2565 (1994).

[35] C. Holland, P. H. Diamond, S. Champeaux, E. Kim, O. Gurcan, M. N. Rosenbluth, G. R. Tynan, N. Crocker, W. Nevins, and J. Candy, Nuclear Fusion **43**, 761 (2003).

[36] C. Hidalgo, M. A. Pedrosa, E. Sánchez, and *et al.*, Plasma Physics and Controlled Fusion **42**, A153 (2000).

[37] S. B. Korsholm, P. K. Michelsen, V. Naulin, J. J. Rasmussen, L. Garcia, B. A. Carreras, and V. E. Lynch, Plasma Phys. Control. Fusion **43**, 1377 (2001).

[38] M. Ramisch, U. Stroth, S. Niedner, and B. Scott, New Jour. Phys. **5**, 12.1 (2003).

Table I. NSTX parameters for shots #113732-113744

| |
|---|
| $R = 0.85$ m |
| $a = 0.68$ m |
| $B_o = 3$ kG |
| $I_p = 0.8$ MA |
| $P_{NBI} = 2 - 4$ MW |
| $T_e(0) = 0.5 - 1$ keV |
| $n_e(0) = 2 - 4 \times 10^{13}$ cm$^{-3}$ |
| $\tau_E \approx 30$ ms |
| $\beta_{\rm tor} \approx 10\%$ |
| $n_e(\text{edge}) \approx 0.2 - 2 \times 10^{13}\text{cm}^{-3}$ |
| $T_e(\text{edge}) = 5 - 50$ eV |
| $L_\perp \sim 2 - 5$ cm |
| $L_\parallel \sim 5$ m |
| $\rho_{\rm s} \sim 0.2$ cm |
| $\beta_{\rm e} \sim 10^{-3}$ |

**Figure Captions:**

1) (Color online) A still-frame 2-D image of $D_\alpha$ light emission from the PSI-5 camera's radial and poloidal $23 \times 23$ cm$^2$ viewing region shown with the positions of the chord data views for shot #113741. The approximate position of the EFIT separatrix is also shown.

2) GPI camera light intensity profiles and the profiles of electron temperature and density from the Thomson scattering diagnostic are shown. The position of the EFIT separatrix is located between $R = 147$ cm and $R = 150$ cm for the thirteen shot series. The approximate position of the separatrix is shown with respect to the radial chord positions. The poloidal chord array (extending up and down from R4) is located slightly outside the separatrix for the shots analyzed in this paper.

3) (Color online) Part (a) shows chord data from the center-most radial GPI chord signal, R4 located at $R \approx 150$ cm. Data from L-mode in the interval $170 - 190.5$ ms and data from H-mode in the interval $190.7 - 200$ ms are used to calculate the bicoherence. The events during $\Delta t \sim 200 - 205$ ms and $\Delta t \sim 214 - 217$ ms are most likely ELM-type events or brief returns to L-mode. (b) FFT power spectrum in time for the center GPI chord signal, R4 (c) $D_\alpha$ trace showing the time of the L-H transition when the amplitude of the trace decreases. The L-H transition time, $t_{LH} = 190.5$ ms, is marked by the dashed vertical line. (d) Power spectrum in time of the Mirnov coil signals.

4) Average FFT power spectra in L-mode and H-mode from chord R4 for a typical NSTX shot, #113741. The power spectra are averaged over $\Delta t \sim 10$ ms intervals during L-mode from $180 - 190.5$ ms and during H-mode from $190.7 - 200$ ms.

5) (Color Online) Contours of the squared bicoherence, $b^2(f_1, f_2)$, equation (2), are shown for six different times before and after the L-H transition for chord R4 during shot # 113739. Time intervals, in ms, are labeled in the upper right corner of each contour. The transition occurs at $t_{LH} \approx 198.5$ ms. Coupling is spread out evenly among all frequencies during L-mode as shown in parts (a) - (d), but is localized to low sum frequencies ($f \leq 100$ kHz ) during H-mode shown in parts (e) and (f). Only values of the $b^2(f_1, f_2)$ that are above the statistical significance level, $1/M \sim 0.06$, are plotted in the contours. The raw chord data for this shot is shown in Fig. 7.

6) The summed bicoherence, $b^2(f_3)$, equation (3), during shot #113739 from chord R4 shows that coupling is spread out among all frequencies during L-mode but is localized to low sum frequencies ($f \leq 100$ kHz ) during H-mode. The curves of $b^2(f_3)$ shown here were calculated from the time window before, $t = 190.3 - 198.4$ ms, and the time window after, $t = 198.6 - 206.7$ ms, the transition. Each time window is divided into 32 records of 128 points each. The statistical significance level is $1/M \approx 0.03$.

7) Part (a) shows chord R4 data from shot #113739. Parts (b) and (c) show the total bicoherence, $b^2(t)$, from equation (4). In (b) the calculation used time windows $\sim$4 ms in length divided into 16 records of 128 points each. The statistical significance level is

$1/M \sim 0.06$. Part (c) shows the same calculation using the same time windows divided into 32 records of 64 points each with $1/M \sim 0.03$. In both cases, no increase in the amount of coupling is seen just prior to the transition.

8) For chord R4, the average total bicoherence, $\overline{b^2(t)}$, equation (5), is calculated for the thirteen shots used in this study. On average, there is no increase in the amount of coupling prior to the L-H transition. The error bars represent the standard error in the mean. Part (a) shows the $\overline{b^2(t)}$ using time windows ∼4 ms in length divided into 16 records of 128 points each, with $1/M \sim 0.06$. Part (b) shows the same calculation the same time windows divided into 32 records of 64 points each, with $1/M \sim 0.03$.

9) Shown here is the average total bicoherence, $\overline{b^2(t)}$ calculated from all thirteen shots, but with better time resolution than shown in figure 8 . The $\overline{b^2(t)}$, using time windows ∼2 ms in length divided into 16 records of 64 points each, shows that there is no increase in the amount of coupling within the 10 ms before the L-H transition.

10) Five of the shots in the series, (# 113732, 113733, 113739, 113741, 113744), had 20 ms or more of L-mode data, and these shots showed an increase in bicoherence long before the L-H transition. Part (a) shows the total bicoherence, $b^2(t)$, for chord R4 during one of these five shots, # 113741. Using time windows ∼4 ms in length with 16 records of 128 points each shows a slight increase nearly 15 ms before the transition. Part (b) shows the average total bicoherence, $\overline{b^2(t)}$, averaged over these five shots shows an increase that is within the R.M.S. error nearly 15 ms before the transition.

11) The poloidal and radial bicoherence profiles of the average total bicoherence, $\overline{b^2(t)}$, are calculated from the five shots with long L-mode portions of data. Part (a) shows that the amount of coupling does not depend on the poloidal position measured from R4. The separatrix is located at $R \approx 150$ cm with a ±3 cm uncertainty. Part (b) shows that the amount of coupling appears to increase with increasing radius. R4 is located at $R \approx 150$ cm.

12) Shown are the results of operating on simple test signals, $x$, where $x$ is a sum of three sinusoids, with a nonlinear function such as $y = x^{\alpha}$ where the nonlinear factor

$\alpha = 0.1 - 2.2$. Part (a) shows the squared bicoherence, $b^2(f_1, f_2)$, evaluated at $f_1 = 220$ Hz and $f_2 = 375$ Hz plotted versus $\alpha$ in the case where the test signal has coupling built into it at $f_1 = 220$ Hz and $f_2 = 375$ Hz and when it is perfectly uncoupled. For $\alpha \neq 1$, the coupling at $b^2(220, 375)$ does not decrease. Part (b) shows the $b^2(t)$ in the coupled and uncoupled cases. When $\alpha \neq 1$, harmonics of $f_1$ and $f_2$ are introduced, even in the uncoupled case, and the total bicoherence increases.

13) The LPC used in the bicoherence code, called BISPEC, suppresses false positives but does not affect bicoherence values associated with actual coupling. Here the total bicoherence is calculated using BISPEC (with and without the LPC) and is compared to the bicoherence calculated using the bispectral analysis routine commercially available for MATLAB for several sections of data from chord R4 (or P4) for shot #113741. The signal left of the first vertical line is not a signal from the plasma; it is background random noise in the system before the gas puff is turned on. The bicoherence calculated in this region of noise is below the significance level when using the LPC.

14) Shown here is the total bicoherence calculated using four perfectly *uncoupled* test signals generated from the sum of three sinusoids. The statistical significance level is the horizontal line. Part (a) shows the effect of a sudden decrease in signal amplitude, as occurs at the L-H transition in GPI chord data. Part (b) shows the effect of a changing mean, $\overline{x}$, in the signal. Part (c) shows the effect of a delta-function type"spike" as might seen in the GPI chord data. Part (d) shows the effect of the signal amplitude increasing or decreasing in an envelope. This is similar to the first $t \sim 5$ ms of chord data when the gas puff is first turned on. The LPC suppresses the artificially high bicoherence values, and data containing events (a) and (c) are avoided in the GPI data when possible.

15) The ratio of the bicoherence to the statistical significance level of a perfectly coupled test signal decreases significantly when the signal to noise ratio (SNR) is below 5. As the SNR decreases, the peak value in the bicoherence for a pair of frequencies is becoming less than unity, even though the signal remains perfectly coupled. Region 1 is deemed unusable because the $b^2(f_1, f_2)$ has been greatly reduced by the noise. Regions 2 and 3 show the SNRs of data that ensure the data are acceptable to use for the bicoherence

calculation. The SNRs in Regions 2 and 3 are typical for GPI chord data from L- and H-mode.

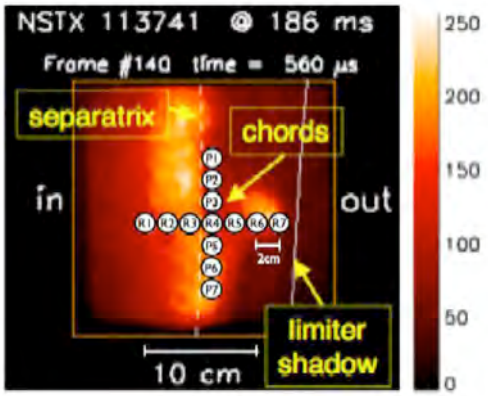
NSTX 113741 @ 186 ms
Frame #140 time = 560 μs
separatrix
chords
in
out
limiter
shadow
10 cm
2cm
250
200
150
100
50
0

FIG. 1:

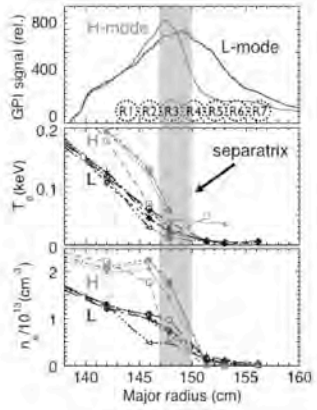
H-mode
L-mode
GPI signal (rel.)
800
400
0
separatrix
H
L
$T_e$ (keV)
0.2
0.1
0
$n_e/10^{13}$(cm$^{-3}$)
2
1
0
140
145
150
155
160
Major radius (cm)

FIG. 2:

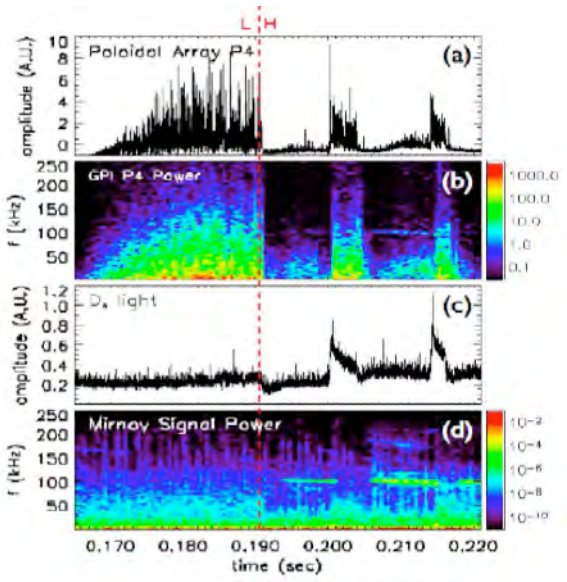
L H
Poloidal Array P4
(a)
amplitude (A.U.)
GPI P4 Power
(b)
f (kHz)
Dα light
(c)
amplitude (A.U.)
Mirnov Signal Power
(d)
f (kHz)
0.170
0.180
0.190
0.200
0.210
0.220
time (sec)

FIG. 3:

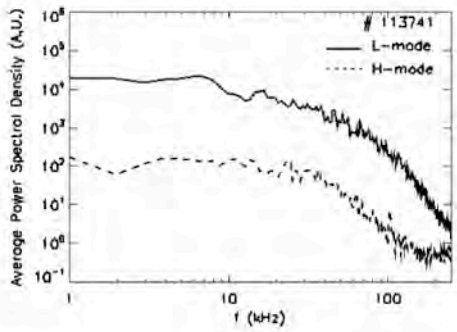
# 113741
L-mode
H-mode
Average Power Spectrol Density (A.U.)
f (kHz)

FIG. 4:

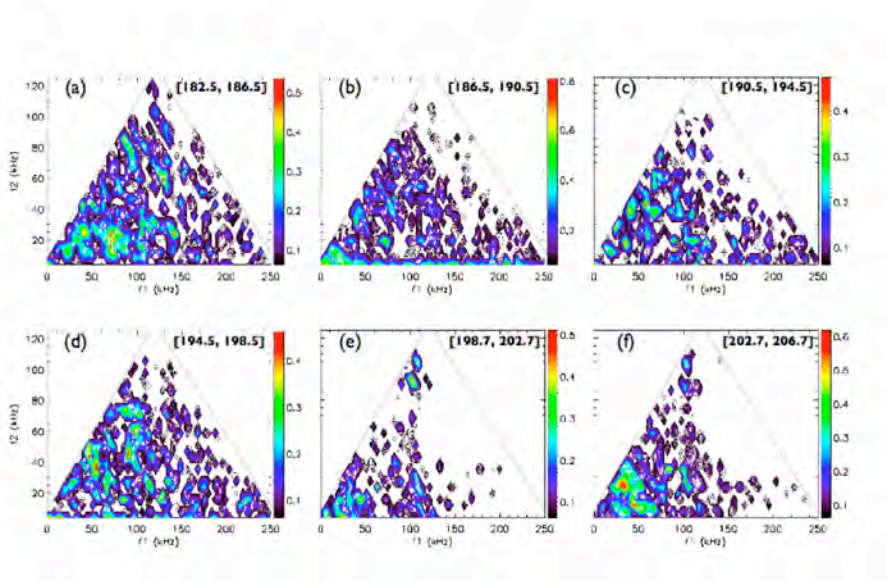
(a) [182.5, 186.5]
(b) [186.5, 190.5]
(c) [190.5, 194.5]
(d) [194.5, 198.5]
(e) [198.7, 202.7]
(f) [202.7, 206.7]
f2 (kHz)
f1 (kHz)

FIG. 5:

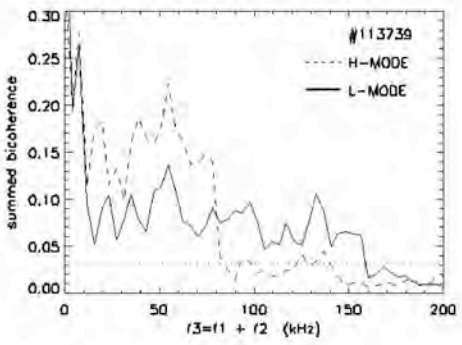
#113739
H-MODE
L-MODE
summed bicoherence
f3=f1 + f2 (kHz)

FIG. 6:

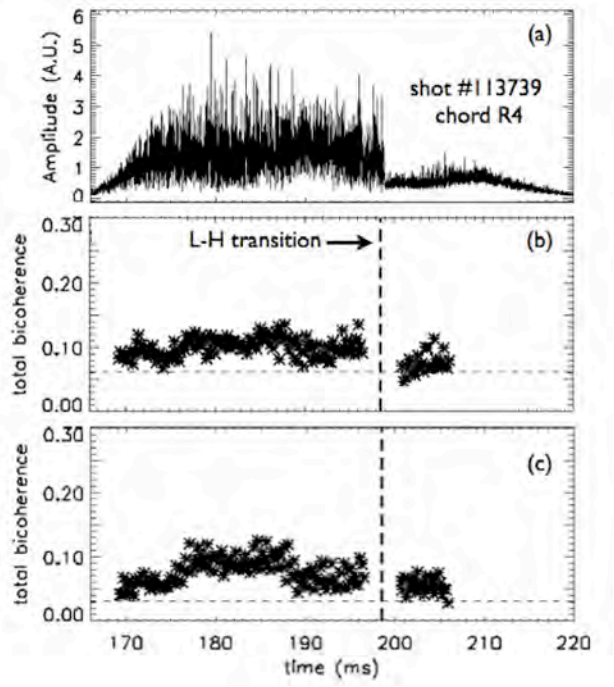


FIG. 7:

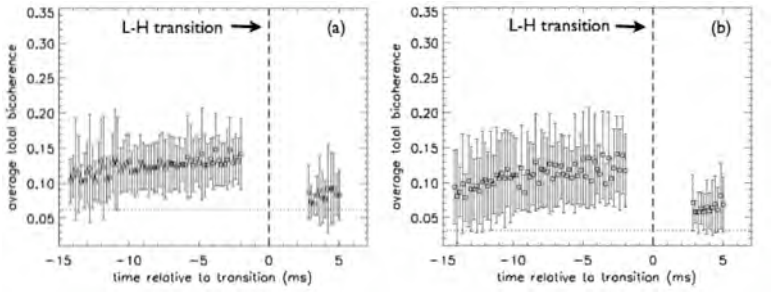


FIG. 8:

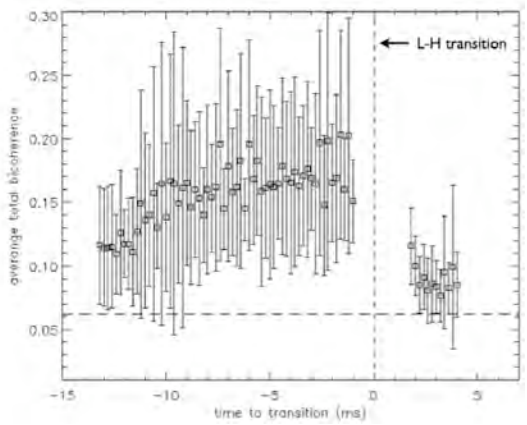


FIG. 9:

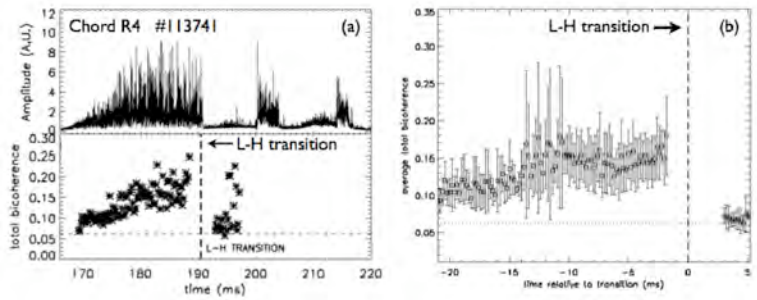


FIG. 10:

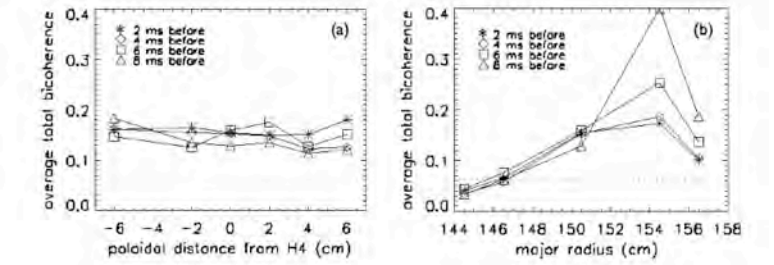


FIG. 11:

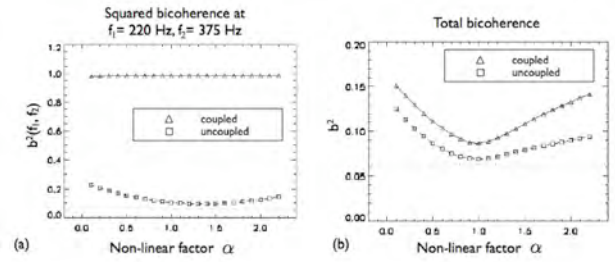


FIG. 12:

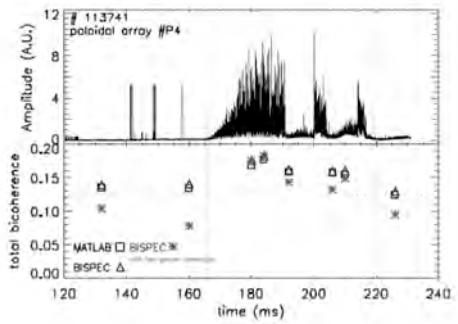


FIG. 13:

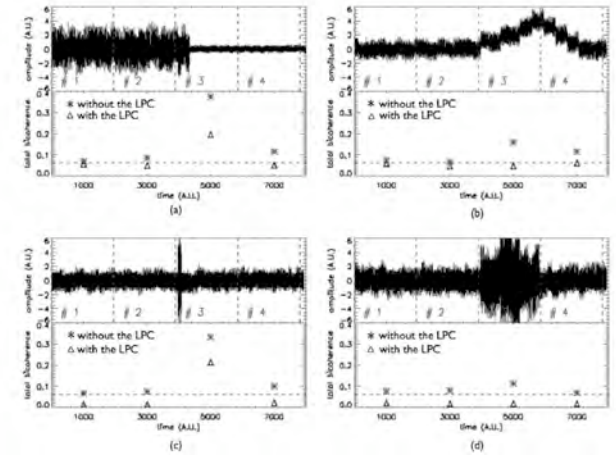


FIG. 14:

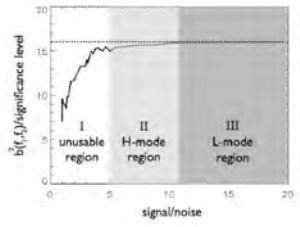


FIG. 15:

# External Distribution

Plasma Research Laboratory, Australian National University, Australia
Professor I.R. Jones, Flinders University, Australia
Professor João Canalle, Instituto de Fisica DEQ/IF - UERJ, Brazil
Mr. Gerson O. Ludwig, Instituto Nacional de Pesquisas, Brazil
Dr. P.H. Sakanaka, Instituto Fisica, Brazil
The Librarian, Culham Science Center, England
Mrs. S.A. Hutchinson, JET Library, England
Professor M.N. Bussac, Ecole Polytechnique, France
Librarian, Max-Planck-Institut für Plasmaphysik, Germany
Jolan Moldvai, Reports Library, Hungarian Academy of Sciences, Central Research Institute for Physics, Hungary
Dr. P. Kaw, Institute for Plasma Research, India
Ms. P.J. Pathak, Librarian, Institute for Plasma Research, India
Dr. Pandji Triadyaksa, Fakultas MIPA Universitas Diponegoro, Indonesia
Professor Sami Cuperman, Plasma Physics Group, Tel Aviv University, Israel
Ms. Clelia De Palo, Associazione EURATOM-ENEA, Italy
Dr. G. Grosso, Instituto di Fisica del Plasma, Italy
Librarian, Naka Fusion Research Establishment, JAERI, Japan
Library, Laboratory for Complex Energy Processes, Institute for Advanced Study, Kyoto University, Japan
Research Information Center, National Institute for Fusion Science, Japan
Professor Toshitaka Idehara, Director, Research Center for Development of Far-Infrared Region, Fukui University, Japan
Dr. O. Mitarai, Kyushu Tokai University, Japan
Mr. Adefila Olumide, Ilorin, Kwara State, Nigeria
Dr. Jiangang Li, Institute of Plasma Physics, Chinese Academy of Sciences, People's Republic of China
Professor Yuping Huo, School of Physical Science and Technology, People's Republic of China
Library, Academia Sinica, Institute of Plasma Physics, People's Republic of China
Librarian, Institute of Physics, Chinese Academy of Sciences, People's Republic of China
Dr. S. Mirnov, TRINITI, Troitsk, Russian Federation, Russia
Dr. V.S. Strelkov, Kurchatov Institute, Russian Federation, Russia
Kazi Firoz, UPJS, Kosice, Slovakia
Professor Peter Lukac, Katedra Fyziky Plazmy MFF UK, Mlynska dolina F-2, Komenskeho Univerzita, SK-842 15 Bratislava, Slovakia
Dr. G.S. Lee, Korea Basic Science Institute, South Korea
Dr. Rasulkhozha S. Sharafiddinov, Theoretical Physics Division, Insitute of Nuclear Physics, Uzbekistan
Institute for Plasma Research, University of Maryland, USA
Librarian, Fusion Energy Division, Oak Ridge National Laboratory, USA
Librarian, Institute of Fusion Studies, University of Texas, USA
Librarian, Magnetic Fusion Program, Lawrence Livermore National Laboratory, USA
Library, General Atomics, USA
Plasma Physics Group, Fusion Energy Research Program, University of California at San Diego, USA
Plasma Physics Library, Columbia University, USA
Alkesh Punjabi, Center for Fusion Research and Training, Hampton University, USA
Dr. W.M. Stacey, Fusion Research Center, Georgia Institute of Technology, USA
Director, Research Division, OFES, Washington, D.C. 20585-1290

The Princeton Plasma Physics Laboratory is operated
by Princeton University under contract
with the U.S. Department of Energy.

Information Services
Princeton Plasma Physics Laboratory
P.O. Box 451
Princeton, NJ 08543

Phone: 609-243-2750
Fax: 609-243-2751
e-mail: pppl_info@pppl.gov
Internet Address: http://www.pppl.gov